PSI-Bericht Nr. 89
Februar 1991

Paul Scherrer Institut

Labor für Werkstoffe und nukleare Verfahren

Temperature Dependence ot the Dynamic Fracture Toughness of the Alloy Incoloy 800 after cold work

K. Krompholz, G. Ullrich

Paul Scherrer Institut
Würenlingen und Villigen
CH-5232 Villigen PSI

Telefon 056/99 21 11
Telex 82 74 14 psi ch
Telefax 056/98 23 27 PSI CH

PSI-Bericht Nr. 89

Temperature Dependence of the Dynamic Fracture Toughness of the Alloy Incoloy 800 after cold work

Temperaturabhängigkeit der dynamischen Bruchzähigkeit an der Legierung Incoloy 800 nach Kaltverformung

K. Krompholz and G. Ullrich
Paul Scherrer Institute
Würenlingen und Villigen
CH-5232 Villigen PSI

Würenlingen und Villigen, Februar 1991

Contents

Precracked charpy-V-notch specimens of the iron-nickel base alloy Incoloy 800 in the as-received condition and after cold work have been tested using an instrumented impact tester (hammer) in the temperature range $293 \leq T/K \leq 1223$. The specific impact energies were determined by dial readings, from the integration of the load versus time and the load versus load point displacement diagrams; in all cases the agreement was excellent.

The specific impact energies and the impulses are correlated with the test temperature and with the degree of cold work, respectively. The dynamic fracture toughness values were determined following the equivalent energy approach.

In all cases a distinct decrease of the mechanical properties in the range between the as-received state and after 5 % cold work was found. The temperature behaviour of the impact energies clearly reveals an increase of its value between room temperature and 673 K. This increase is distinctly reduced after cold work. The dynamic fracture toughness decreases with increasing temperature.

The fracture surfaces clearly show elasto-plastic fracture behaviour of the material in the temperature regime investigated.

Angerissen ISO-V-Proben der Eisen-Nickel-Basis-Legierung Incoloy 800 im Anlieferungszustand und nach Kaltverformung wurden mit Hilfe eines instrumentierten Pendelschlagwerkes im Temperaturintervall $293 \leq T/K \leq 1223$ untersucht. Die spezifischen Schlagenergien wurden mit Hilfe des Schleppzeigers, der Integration des Kraft-Zeit- und des Kraft-Weg-Diagrammes ermittelt. In allen Fällen war die Uebereinstimmung ausgezeichnet.

Die spezifischen Schlagenergien und die Impulse wurden sowohl mit der Versuchstemperatur als auch mit dem Verformungsgrad korreliert. Die dynamische Bruchzähigkeit wurde mit Hilfe der äquivalenten Energie-Näherung ermittelt.

In allen Fällen wurde ein deutliches Absinken der mechanischen Eigenschaften zwischen dem Anlieferungszustand und 5 % Kaltverformung gefunden. Die Temperaturabhängigkeit der Schlagenergien zeigt einen deutlichen Anstieg der Werte zwischen Raumtemperatur und 673 K. Dieser Anstieg wird nach Kaltverformung deutlich reduziert. Die dynamische Bruchzähigkeit sinkt mit steigender Temperatur.

Die Bruchflächen zeigen klar das elasto-plastische Bruchverhalten des Materials im untersuchten Temperaturbereich.

1 Introduction

Incoloy 800 is basically an austenitic iron-nickel-chromium alloy containing relatively minor but important amounts of carbon, aluminium, and titanium. Alloys of this general type have found wide application in many high-temperature engineering fields, particularly in industrial heating for furnace equipment and electrical elements; in the petro-chemical industry for piping systems, cracker tubes and reformers; and in power generation for boiler tubes.

It is also under general consideration for nuclear applications for pressure vessels, heat-exchanger and steam-generator tubing, and ducting.

The wide variety of applications of this material are established by providing a favourable combination of mechanical strength and corrosion resistance, which makes it useful for components operating at temperatures up to 1073 K (about 800 °C).

In all cases cold deformation is an important factor influencing the mechanical properties and the structural stability of this material. For this reason a test program is considered in which at different specimen types and material states material data could be obtained which would be part of a basic safety program. An important question is the structural stability and the influence of cold working on the mechanical properties. For the material 1.4876 after cold work and following ageing in the temperature range $823 \leq T/K \leq 923$ a minimum in ductility was observed. Quantitative specifications of the exact position of the rest ductility dependend on ageing time; the degree of deformation and chemical composition should be elaborated as far as possible.

In this contribution the results of tensile test on cold worked material at room temperature, as well as on charpy impact tests on different predeformed materials at different temperatures are reported, the main consideration here is the cold work and the temperature.

2 Material Properties

The material under investigation is the alloy

X 10 NiCrAlTi 3220 (Ferrotherm 4876),

material number 1.4876.

The material was delivered in the form of plates, 28 mm thick, by Krupp Suedwestfalen AG, Werksgruppe Siegen and was sent to this institute by Hochtemperatur-Reaktorbau, Mannheim, as material for these investigations.

The chemical composition and the mechanical properties from the supplier's certificate is given in Table 1.

The narrow scatter band shows the homogeneity of the delivered plates.

3 Experimental Procedures

3.1 Cold Work

Some strips were taken from the plates and were cold deformed by hammers. The degree of cold work was chosen to be 5 %, 10 %, and 25 %.

3.2 Tensile Tests

The tensile specimens (Type B 5 x 50, DIN 50125), see Fig. 1, for these investigations were taken with the axial direction parallel to the rolling direction of the plates. For the strips to be cold worked the rolling direction was marked.

The tensile tests were perfonned on a screw-driven electromechanical test machine of the supplier Contraves, Type ZM 50 A according to DIN 50145. The results are also necessary for prefatiguing the impact speciman in a suitable manner. The results are presented in Table 2.

3.3 Prefatigue

The charpy-V-notch (ISO-V-) specimens, see Fig. 2, were taken from the plate and strips with the notch direction T-L [1]. Some specimens were polished at the surfaces perpendicular to the notch in order to get a good observation of the running crack during fatigue. The specimens were fatigued on an electromechanical high frequency pulsator, type HFP5000, delivered by Roell and Korthaus, Amsler, Merishausen, Switzerland, in compression. For the chosen parameters the frequency regime was found.

$149 \geq f/Hz \geq 110$

After determining the selected crack length observed on the surfaces optically the lower frequency of 110 Hz was used as the lower limit. Reaching this lower limit the test machine stops automatically. This prefatigue procedure delivers highly reproducable crack lengths. A part of these specimens were taken for thermal ageing in the furnaces.

3.4 Impact Testing

The impact machine used for these experiments is described in detail elsewhere [2]. An automatic centering device with a cooling chamber and a resistance furnace was adapted for use on the impact machine; for temperature dependent toughness determinations. The test temperatures $293 < T/K \leq 1223$ were obtained by heating the specimens in the resistance furnace for approximately $1.32\ 10^3$ s for the temperatures up to 1073 K and only 900 s for higher temperatures. The temperatures were measured using calibrated Chromel-Alumel thermocouples.

After heating, the specimens were pushed to the anvil of the impact machine, with the centering device and 4 seconds later impact occured. The experimental detail is described elsewhere [3].

After fracture of the specimen, the length of the fatigue crack was measured by means of a microscope, and from that, the specimen geometry, the load, and the dynamic properties could be determined.

4 Reduction of Data

For the determination of the prefatigue data, tensile tests on the cold worked material were performed. The results are presented in Table 2. They clearly show that the 0.2 flow stress increases significantly with the degree of deformation, where the degree of deformation is

$$V = \frac{d_0 - d}{d_0} \cdot 100 = \frac{\Delta d}{d_0} \cdot 100, \tag{1}$$

where d_0 is the initial thickness of the plate and d the final thickness after cold working.

For prefatigue the following conditions have to be fullfilled [4]

$$P_L = \frac{4}{3} \cdot \frac{B(w-a)^2 Rp_{0.2}}{s}, \tag{2}$$

where P_L is the limit load, B the thickness of the specimen, s = 4w the span, w the width of the specimen, a = the crack length and $Rp_{0.2}$ the 0.2 % flow stress. This result is obtained by the calculation of the pure bending stress.

It must be considered that

- only fractions of the limit load are applied. In the start up phase for P_{max}

$$P_{max} < 0.7 P_L \tag{3}$$

  was selected.

- the last 0.6 mm were prefatigued with a maximum load of

$$P_{max} = 0.4 P_L, \tag{4}$$

These conditions could be fulfilled in nearly all cases. In all cases very fine fatigue cracks with very small plastic zones were obtained. The data are presented in Table 3. The maximum stress intensity was calculated according to

$$K_{max} = \frac{P_{max} \cdot s}{B \cdot w^{3/2}} \cdot f\left(\frac{a}{w}\right). \tag{5}$$

with

$$f(\frac{a}{w}) = \frac{3(\frac{a}{w})^{1/2}\{1.99 - (\frac{a}{w})(1 - \frac{a}{w})(2.15 - 3.93(\frac{a}{w}) + 2.70(\frac{a}{w})^2)\}}{2(1 + 2\frac{a}{w})(1 - \frac{a}{w})^{3/2}} \tag{6}$$

The absorbed impact energy can be determined from the load versus load point displacement diagram by

$$E(4) = \int_0^{V_{LL,max}} P d_{V_{LL}}, \tag{7}$$

where P is the load and V_{LL} the load point displacement. The upper limit $V_{LL,max}$ means the complete load point displacement during impact. If $E^m(4)$ is needed, the upper limit is V_{LL} corresponding to the maximum load.

Impact energies can also be calculated from the load versus time diagram using the following equation

$$I = \int_0^t P dt = m(V_0 - V_t), \tag{8}$$

where V_0 is the velocity of the hammer immediately prior to impact, m the mass, V_t the velocity at the time t, P the force and t is the time elapsed after initial contact between specimen and tup. I^m is obtained by using the time up to the load maximum, during integration of the load versus time diagram.

By definition

$$E_a := V_0 \int_0^t P dt, \tag{9}$$

and by simple rearrangement the following equation is obtained [4]

$$E(3) = E_a \left\{ 1 - \frac{E_a}{4E(0)} \right\}. \tag{10}$$

where V_0 (is kept constant in equation (9)) with 4.98 m/s, E(0) is the maximum energy obtainable from the hammer before impact and is kept constant with E(0) = 225 J. After final fracture, the amount for the average crack extension caused by pre-fatiguing was determined optically and the crack length was calculated according to

$$< a >= \frac{1}{10} \left\{ \frac{a_0 + a_{10}}{2} + \sum_{i=1}^{9} a_i \right\}. \tag{11}$$

where a_0 and a_{10} are the crack lengths at the surface of the specimen and a_i characterizes the amount of crack length in evenly spaced measurement points from one side of the specimen to the other across the crack front.

For these types of load versus load point displacement diagrams it is proposed to determine the fracture toughness following the equivalent energy approach [6, 7]. Simple geometrical considerations show that P_Q can be calculated according to

$$P_Q = \sqrt{2 \cdot A \tan \alpha}, \tag{12}$$

where A is the area of the load versus load point displacement diagram up to the maximum load ($A = E^m(4)$) and $\tan\alpha$ is the slope of the "elastic region" of the diagram. This is described in more detail elsewhere [3, 6].

5 Experimental Results

The cold work dependence of the yield strength and the ultimate tensile strength is presented in Fig. 3, while the reduction of area after fracture Z and the percentage elongation after fracture A_{10} is shown in Fig. 4. The temperature dependence of the impact energy evaluated from the different equations (7) and (10) as well as from the dial reading is given in Figs. 5 and 6. The temperature dependence of the impact energies up to the load maximum during impact E^m is presented in Figs. 7 and 8. The

impulse during impact as a function of temperature is shown in Figs. 9 and 10, while the impact up to the load maximum is presented in Figs. 11 and 12. The temperature dependence of the stress intensity factor evaluated due to the equivalent energy approach is shown in Figs. 13 and 14. All the isothermes of the parameters described before as a function of cold deformation are presented in Figs. 15 to 19.

6 Discussion

As pointed out earlier [3, 5 - 7] the absorbed impact energy determined from the dial readings of the pendulum, from the load versus time diagrams and the application of equations (9) and (10), which delivers E(3), and the impact energies determined by the integration of the load versus load point displacement diagram using equation (7), are in good agreement. The signals are stored by a recorder, Type Nicolet Model 206 with a memory of 4096 12 bit words, time sequence 5 μs. In all cases the impact energies are normalised to the remaining ligament.

The normalised impact energies show a maximum in the regime of 573 K (300 °C) if the temperature dependence of the as-received material is considered. If the temperature of 673 K (400 °C) is exceeded a steep decrease is found up to 1173 K (900 °C). At 1223 K a slight increase is observed. The maximum of the impact energies is shifted to higher temperatures if the degree of cold work is considered. The maximum is lowered and if 25 % cold work is regarded there is nearly no temperature dependence in the impact energy (see Figs. 5 and 6). The temperature dependence of the energy up to the load maximum E^m decreases with increasing temperature for the as-received state, while there is no pronounced temperature dependence found for the cold-worked specimens (Figs. 7 and 8). The impulses during impact (Figs. 9 - 12) clearly exhibit the same tendency as found for the impact energies reported before. These results are expected because the impulse is the basis for the calculation of the impact energy from the load versus time diagram according to equations (9) and (10). The temperature dependence of the somewhat artificial parameter K reveals a decrease with increasing temperature. A small maximum is found at 973 K (700 °C). The decrease of K is also lowered with an increasing degree of deformation of the material.

The isothermes of the impact energies E as a function of the degree of deformation reveal

a decrease in the impact energy with increasing degree of cold work. An intermediate maximum is found at 623 K (400 °C). The decrease in impact energy is lowered with increasing temperature as can be seen in Fig. 15, Fig. 16 shows the cold-work dependence of the energy up to the load maximum which exhibit the same tendency. For the cold-work dependence of the impulses which are derived from the load versus time diagrams, the same tendencies are found. The intermediate maxima are more pronounced in all cases (see Figs. 17 and 18).

The cold-work dependence of the stress intensity (dynamic fracture toughness) reveals an intermediate maximum at 10 % cold work, if the isothermes at room temperature and 673 K (400 °C) are regarded. This maximum is shifted towards 5 % cold work if 1173 K (900 °C) and 1223 K (950 °C) is observed. The main tendency follows the impact energy; with increasing degree of cold work the fracture toughness decreases.

In principal it is expected that 5 % cold deformation is reached in manufacturing tubes and other components. The results presented here clearly exhibit that a cold work leads to the tendency of material weakness with respect ot the mechanical properties.

7 Conclusion

Instrumental impact tests were performed on prefatigued charpy-impact tests specimens of the material Incoloy 800 in the as-received state and after 5 %, 10 % and 25 % cold work in the temperature range $293 \leq T/K \leq 1223$. The impact energies were determined with different methods, the agreement was excellent.

The temperature dependence of the impact energies exhibit an intermediate maximum at 673 K (400 °C). This maximum is more or less suppressed with increasing cold work.

The temperature dependence of the fracture toughness reveals a decrease with increasing temperature. The decrease is most pronounced in the as-received state.

The isothermes of the impact energies as a function of cold work show that between the as-received state and 5 % cold work a large decrease in the energy can be observed. This is very strongly pronounced at room temperature and at 673 K (400 °C). In this region the usual degree of cold work can be found manufacturing components. From

this point of view a weakness of the material with respect to its mechanical properties can be expected.

Acknowledgment

The authors are grateful to Mr J. Kamber who performed these experiments.

References

[1] Standard Test Method for Plane-Strain Fracture Toughness of Metallic Materials. Annual Book of ASTM Standards, Sect. 3, Vol. 03.01 1987, Designation E 399-83, 670-715

[2] J. Kamber, W. Bulgheroni, A. Christen. Das instrumentierte Pendelschlagwerk-Weiterentwicklung eines Werkstoffprüfgerätes für den Einsatz in Hotzellen. EIR-Bulletin 58, Mai 1986, 5 - 9

[3] K. Krompholz, G. Ullrich. Temperature Dependence of the Dynamic Fracture Toughness and the Specific Impact Energies of the Alloy Nimonic 86.
Mat.-wiss. u. Werkstofftech. 19 (1988) 143 - 151

[4] Loc. cit. [1]. Standard Test Method for J_{IC}. A Measure of Fracture Toughness. Designation E 318 - 87, 968 - 990.

[5] K. Krompholz, P. Tipping, G. Ullrich, Results from Investigations with an Instrumented Impact Machine on a Molybdenum Base Alloy, Nickel Base Alloys, and Incoloy 800
Z. Werkstofftech. 15 (1984) 117 - 123

[6] K. Krompholz, P. Tipping, G. Ullrich. Investigations into the Influence of the Tup Velocity and the Heat Treatment on the Dynamic Fracture Toughness of Inconel 625.
Z. Werkstofftechn. 15 (1984) 199 - 206

[7] K. Krompholz, G. Ullrich. Investigation of the Influence of Impact Velocity and Temperature on the Dynamical/Mechanical Properties of the Material 22 NiMoCr 37.
Journal of Testing and Evaluation 16 (1988) 205 - 213

Table 1 Chemical Composition and Mechanical Properties of the Alloy Incoloy 800

Tabelle 1 Chemische Zusammensetzung und mechanische Eigenschaften der Legierung Incoloy 800

C	Si	Mn	P	S	Cr	Ni	Al	Ti	N
0.045	0.64	1.03	0.014	0.007	20.05	30.77	0.169	0.28	0.0200

Specimen Dimension Probenabm. (mm)	$Rp_{0.2}$/MPa	$Rp_{1.0}$/MPa	R_m/MPa	Ag/%	Z/%	A_V/Joule ISO-V
Ø 10	183	217	534	49	68	268, 286, 282
Ø 10	194	227	535	51	71	230, 239, 240

$Rp_{1.0}$ 1.0 % Strength / 1% Dehngrenze
$Rp_{0.2}$ Yield Strength / Streckgrenze
R_m Ultimate Tensile Strength / Bruchfestigkeit
Ag Percentage Elongation after Fracture / Prozentuale Dehnung nach dem Bruch
Z Reduction of Area after Fracture / Brucheinschnürung

Table 2 Measured Data from the Tensile Test of the Alloy Incoloy 800 with different degrees of cold-work

Tabelle 2 Gemessene Zugversuchsdaten der Legierung Incoloy 800 mit unterschiedlichen Graden von Kaltverformung

Degree of cold-work V/%	$Rp_{0.2}$/MPa	R_m/MPa	A_{10}/%	Z/%	
0	203^{+21}_{-15}	497^{+5}_{-4}	48.7±1,2	74±1	(1)
5	391^{+8}_{-5}	537^{+2}_{-4}	34.0±2	73±2	(1)
10	424±2	546±7	32.0±4	73±1	(1)
25	533^{+11}_{-11}	590±13	15±3	71±2	(2)

(1) three specimens
(2) six specimens

Table 3 Limit Load and maximum Load during prefatigue of Incoloy 800 with different degrees of cold-work

Tabelle 3 Grenzlast und maximale Last während des Anschwingens von Incoloy 800 mit unterschiedlichen Graden von Kaltverformung

Degree of cold-work $V=100\cdot\frac{\Delta d}{d_0}$/%	$Rp_{0.2}$/MPa	a/mm	P_L/kN	P_{max}/kN	P_{max}/P_L
0	202^{+21}_{-15}	4.2	2.265	1.614	0.713
		5.0	1.683	0.914	0.543
5	391^{+8}_{-5}	4.4	4.087	2.093	0.512
		5.0	3.258	1.046	0.321
10	424±2	4.4	4.432	2.274	0.513
		5.0	3.533	1.137	0.322
25	533±11	4.4	5.572	2.859	0.513
		5.0	4.442	1.429	0.322

Fig. 1 Tensile specimens according to DIN 50125
Abb. 1 Zugproben nach DIN 50125

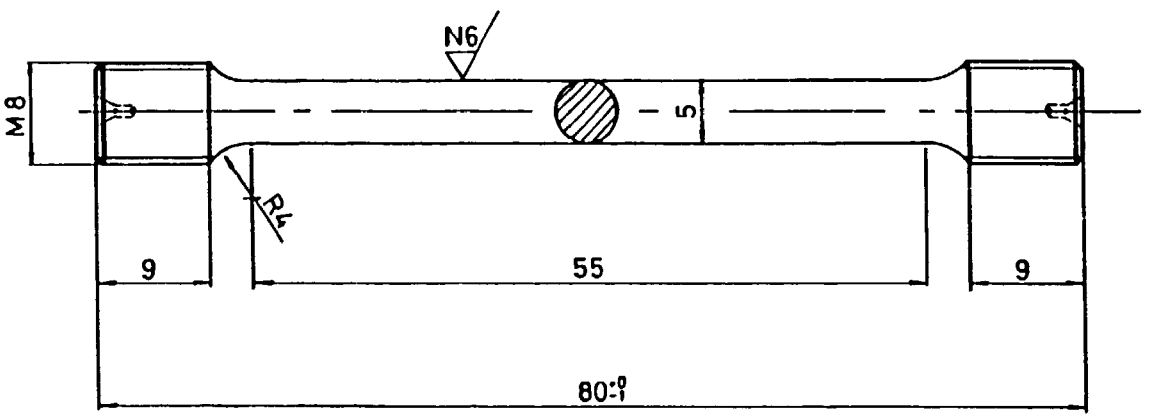

Fig. 2 ISO-V-Specimens (Dimensions in mm)
Abb. 2 ISO-V-Proben (Dimensionen in mm)

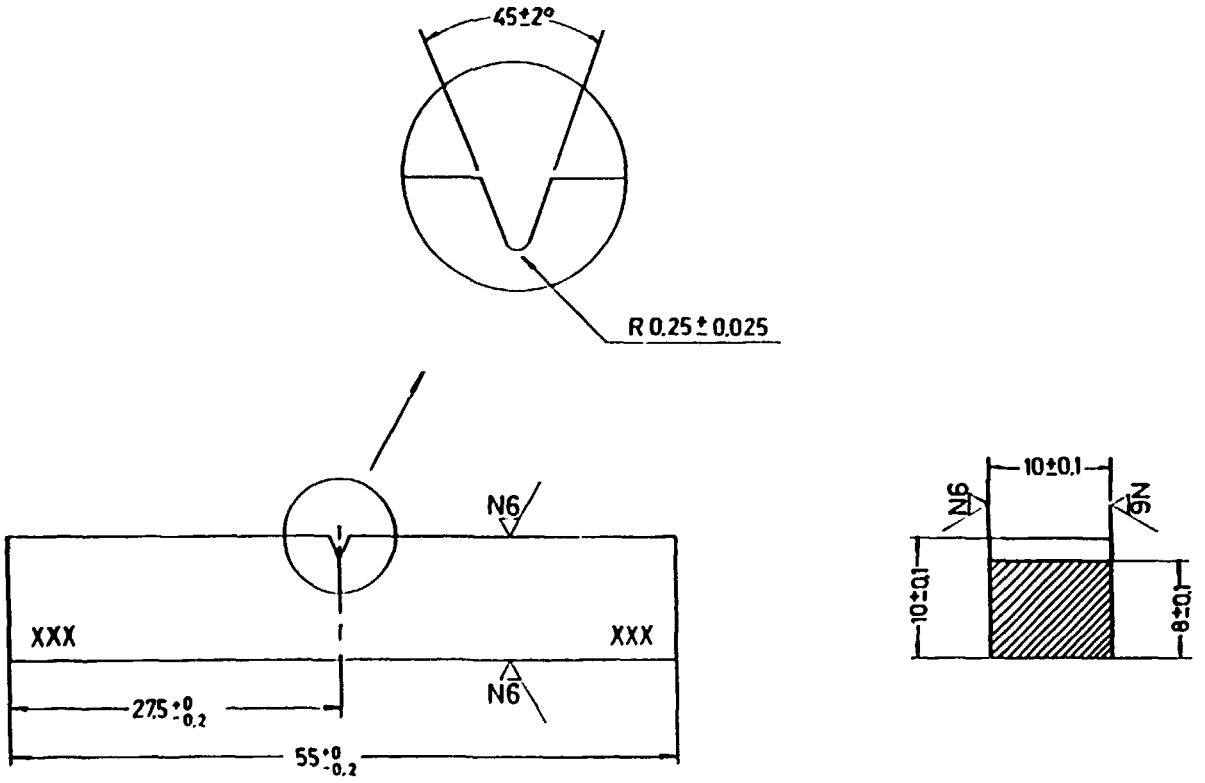

Fig. 3 Yield Strength and Ultimate Tensile Strength as a function of cold-work

Abb. 3 Streckgrenze und Zugfestigkeit als Funktion der Kaltverformung

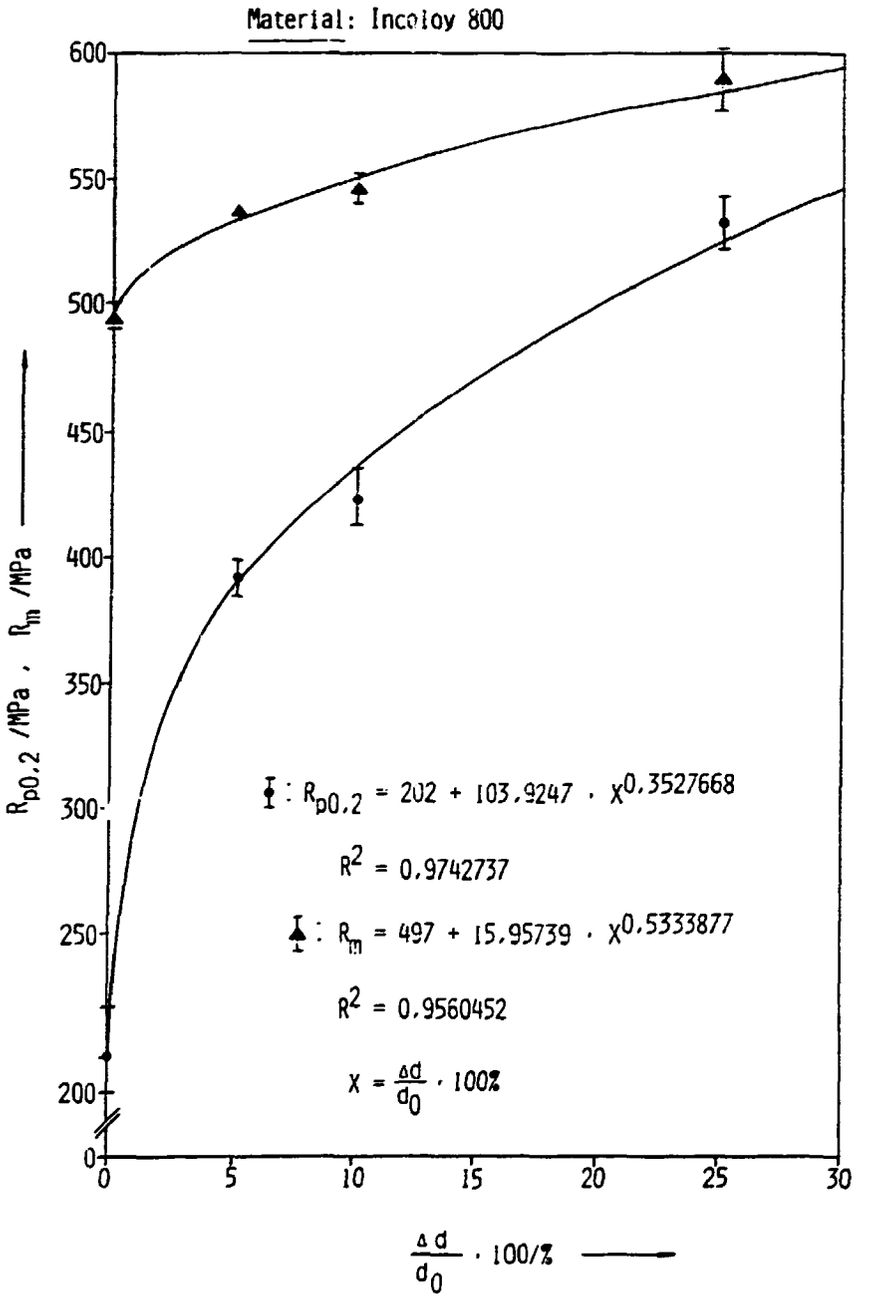

Fig. 4 Reduction of area Z and percentage elongation after fracture A_{10} as a function of cold-work

Abb. 4 Einschnürung Z und prozentuelle bleibende Dehnung nach dem Bruch A_{10} als Funktion der Kaltverformung

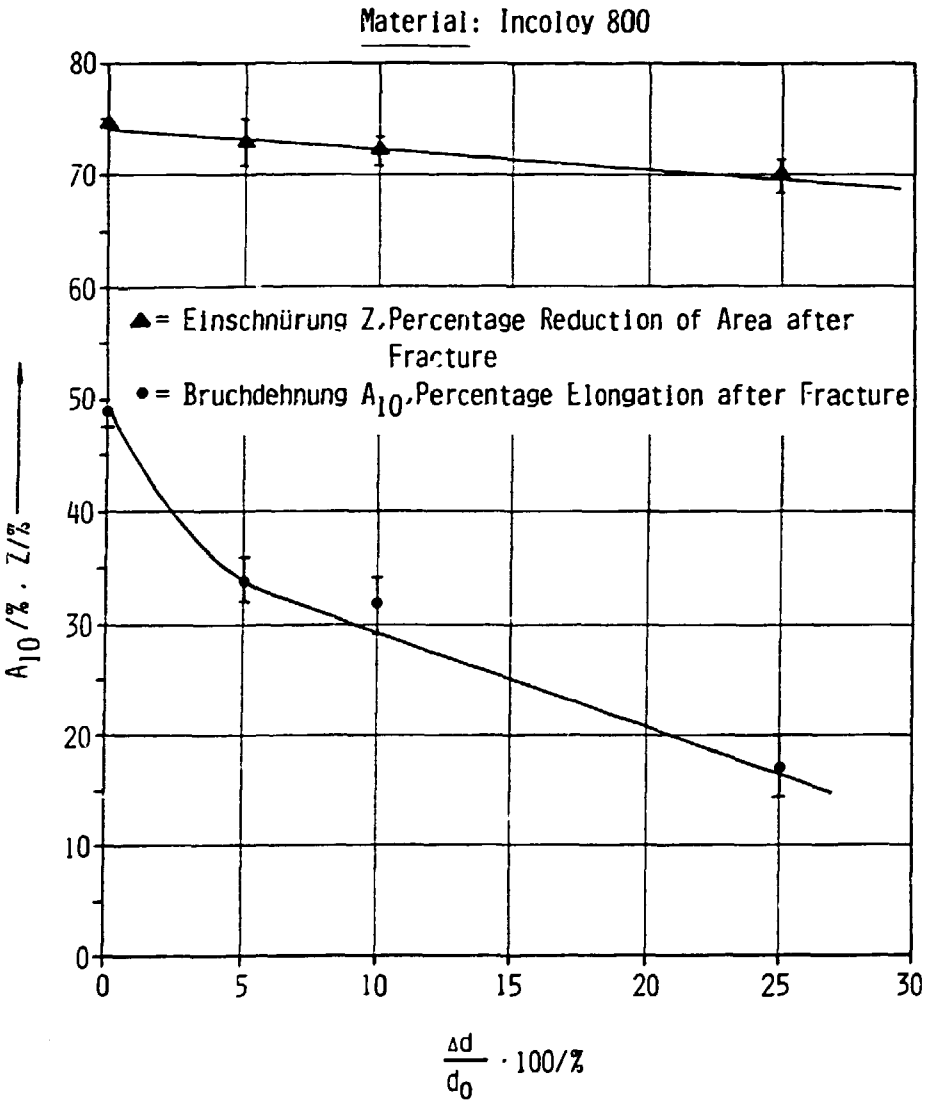

Fig. 5 Temperature Dependence of the normalized Impact Energy E for the as-received state and the 5 % cold-work

Abb. 5 Temperaturabhängigkeit der normalisierten Schlagenergie E für den Anlieferungszustand und nach 5 % Kaltverformung

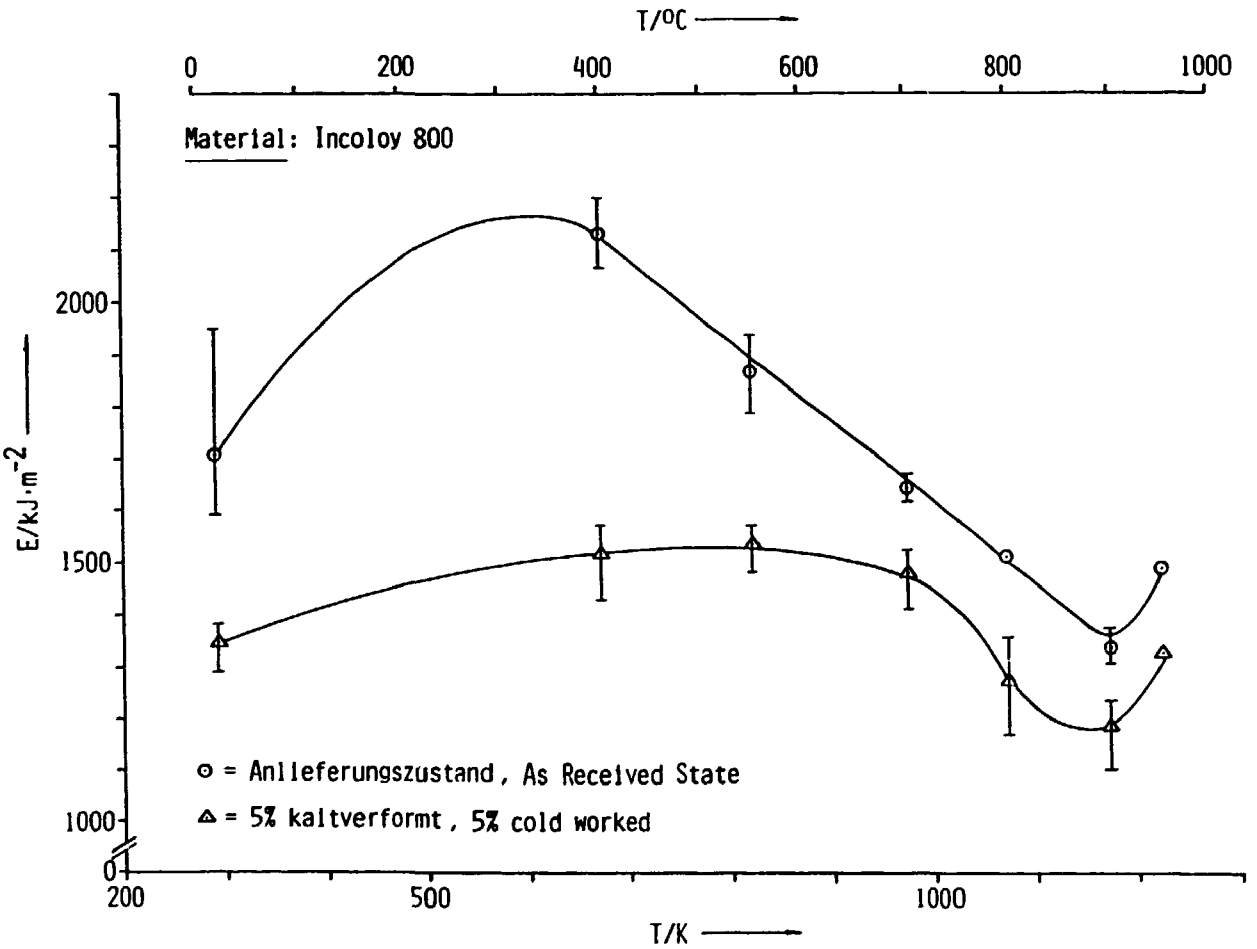

Fig. 6 Temperature Dependence of the normalized Impact Energy E for the 10 % and 25 % cold-work

Abb. 6 Temperaturabhängigkeit der normalisierten Schlagenergie E nach 10 % und 25 % Kaltverformung

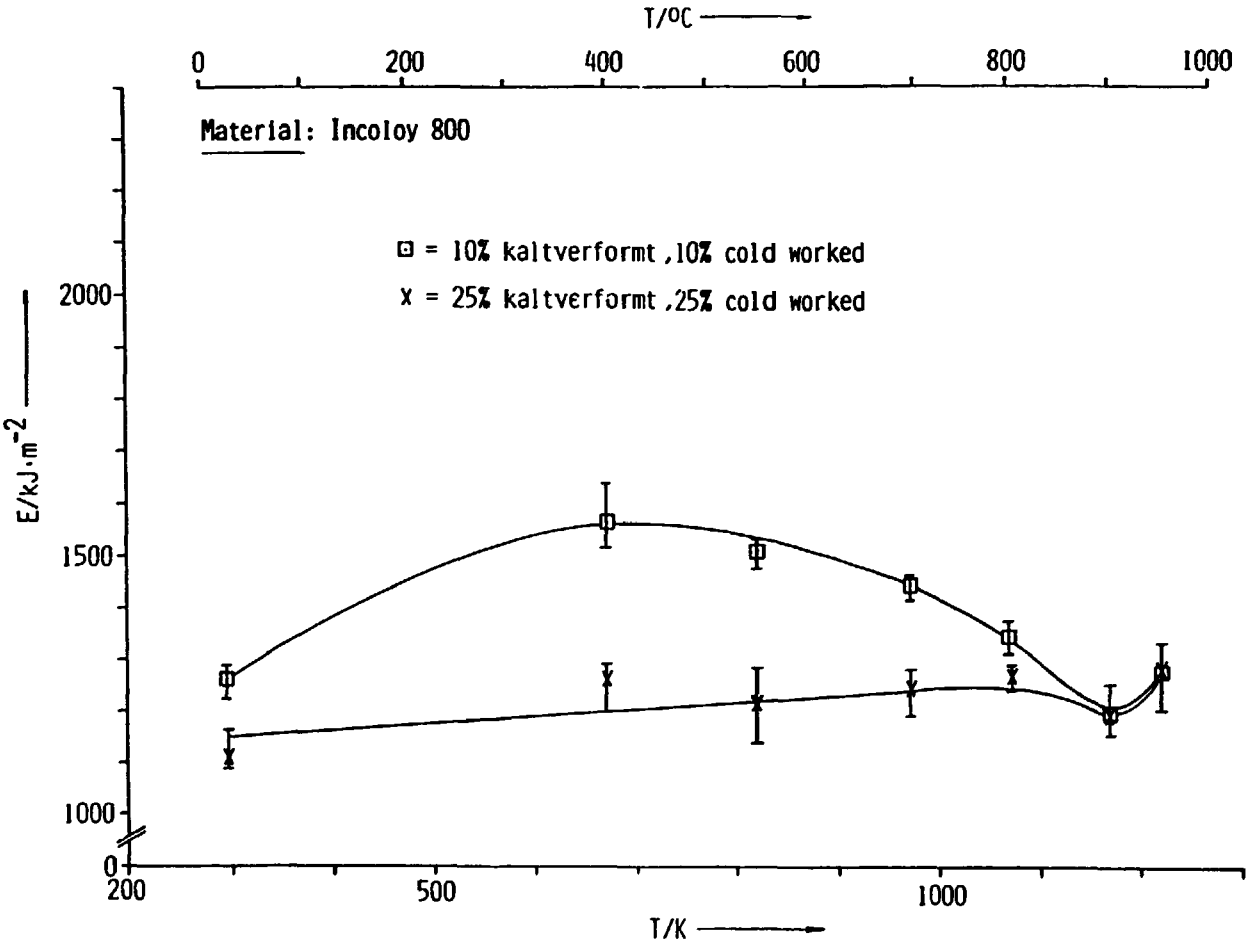

Fig. 7 Temperature Dependence of the normalized Energy up to the Load Maximum E^m for the as-received state and the 5 % cold-work

Abb. 7 Temperaturabhängigkeit der normalisierten Energie bis zum Lastmaximum E^m für den Anlieferungszustand und nach 5 % Kaltverformung

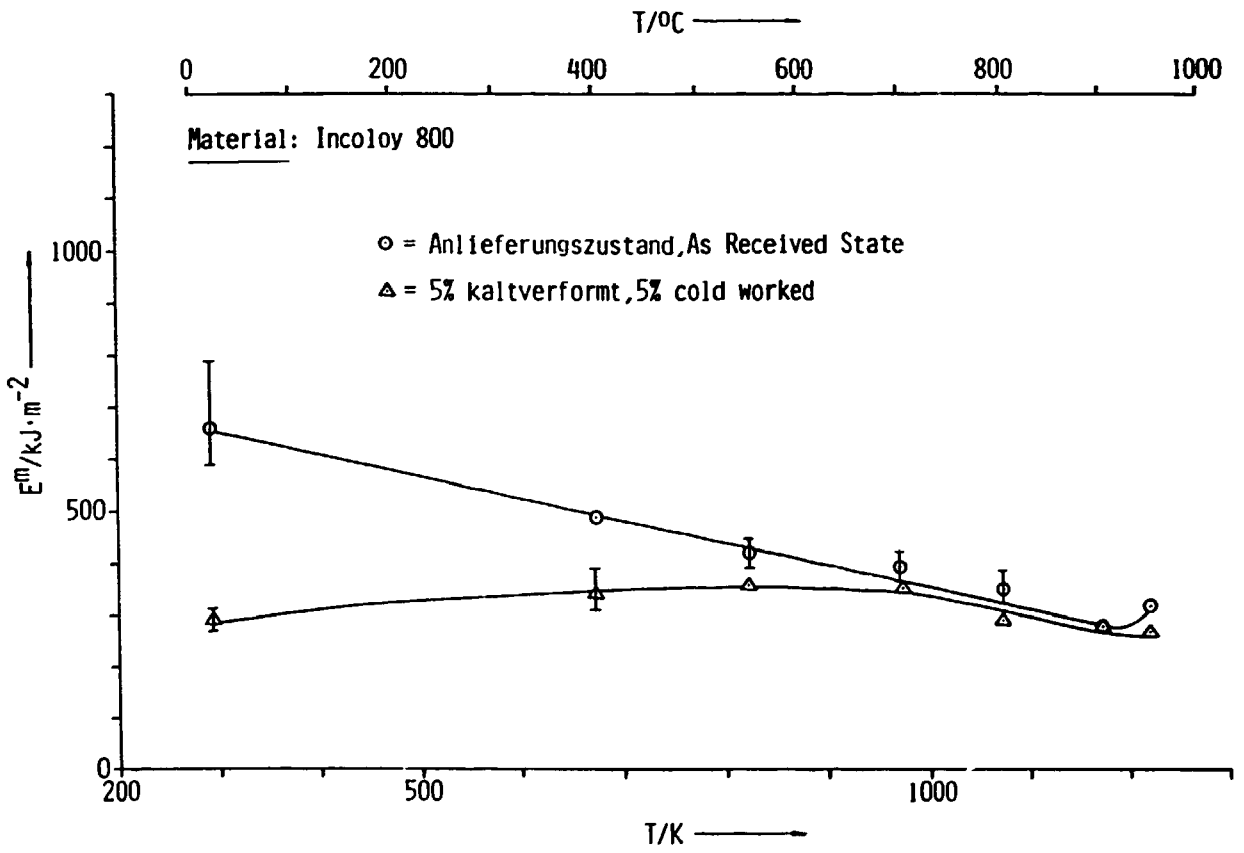

Fig. 8 Temperature Dependence of the normalized Energy up to the Load Maximum E^m for 10 % and 25 % cold-work

Abb. 8 Temperaturabhängigkeit der normalisierten Energie bis zum Lastmaximum E^m für 10 % und 25 % Kaltverformung

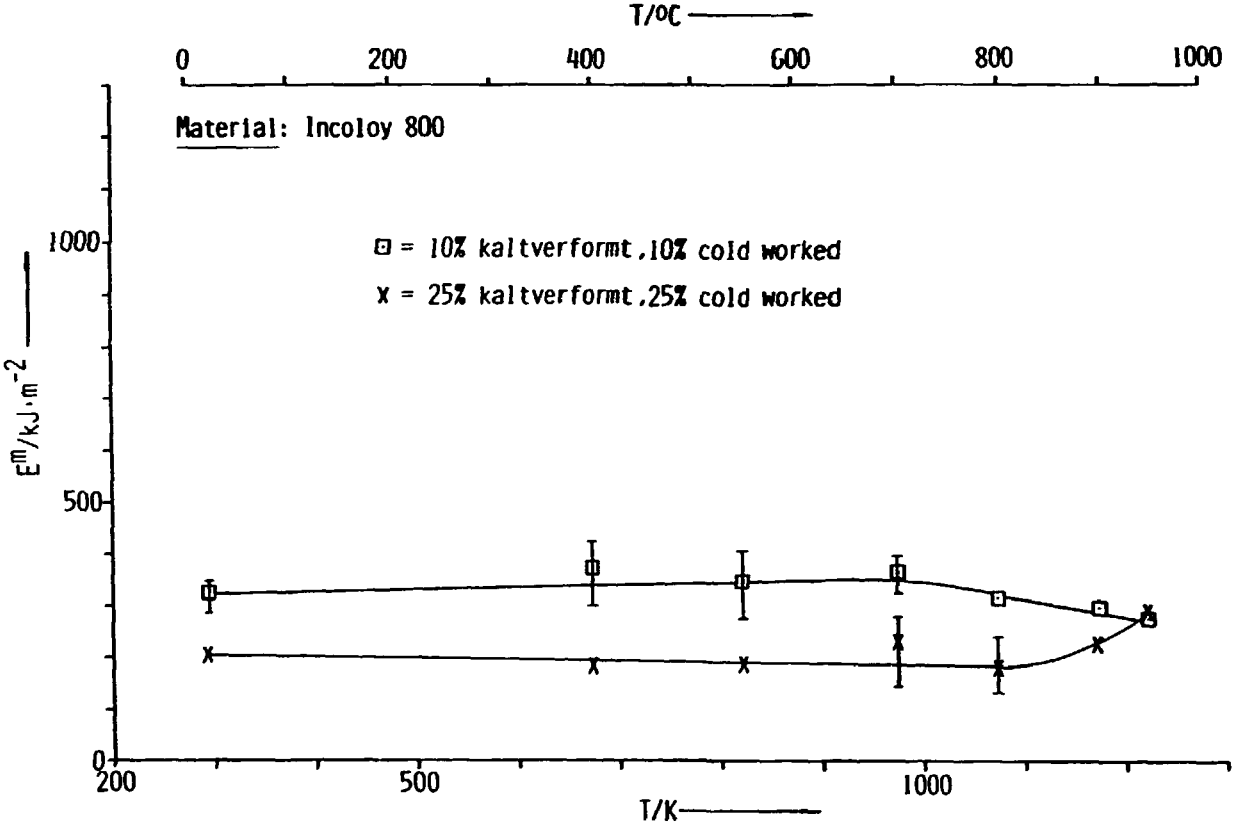

Fig. 9 Temperature Dependence of the Impulse I for the as-received state and the 5 % cold-work

Abb. 9 Temperaturabhängigkeit des Impulses I für den Anlieferungszustand und nach 5 % Kaltverformung

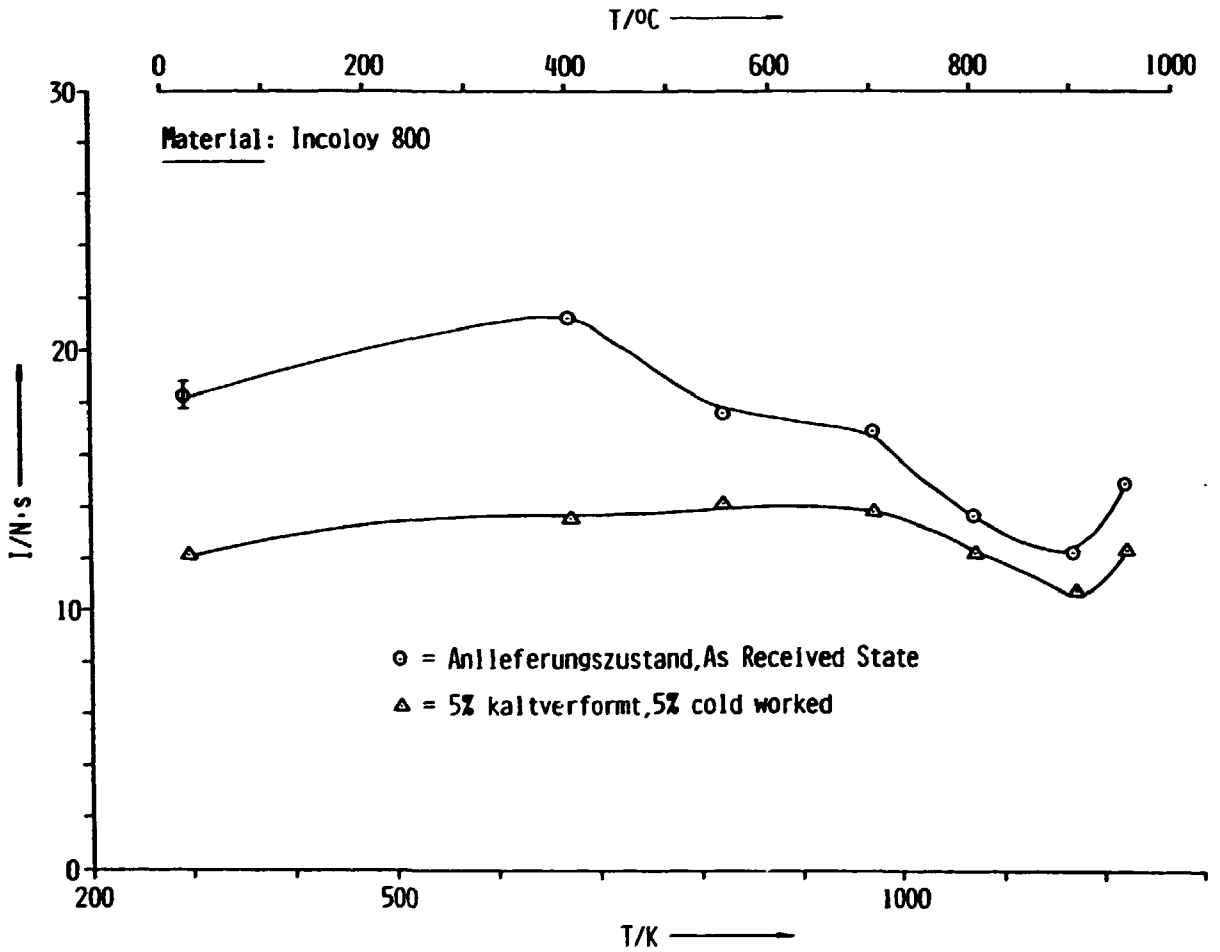

Fig. 10 Temperature Dependence of the Impulse I for the 10 % and 25 % cold-work

Abb. 10 Temperaturabhängigkeit des Impulses I für 10 % und 25 % Kaltverformung

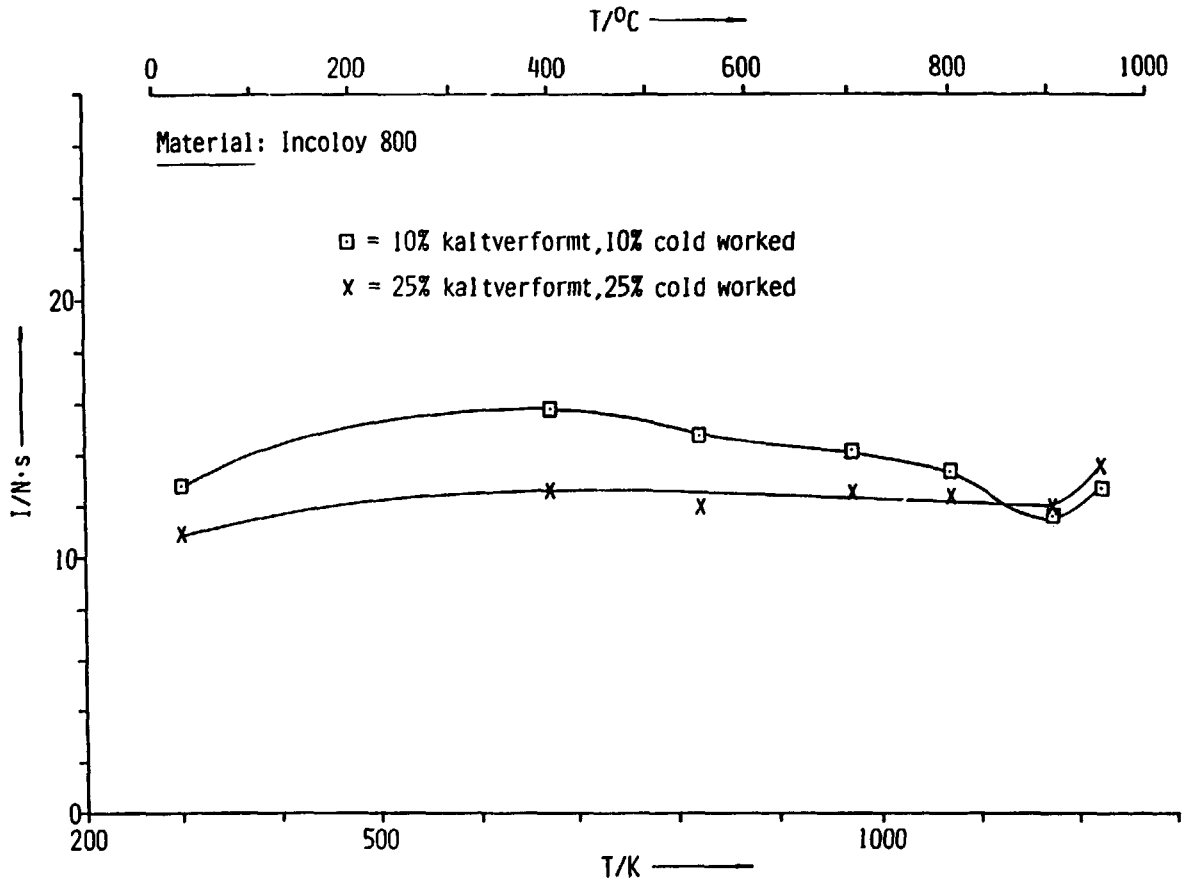

Fig. 11 Temperature Dependence of the Impulse up to the Load Maximum I^m for the as-received state and 5 % cold-work

Abb. 11 Temperaturabhängigkeit des Impulses bis zum Lastmaximum I^m für den Anlieferungszustand und nach 5 % Kaltverformung

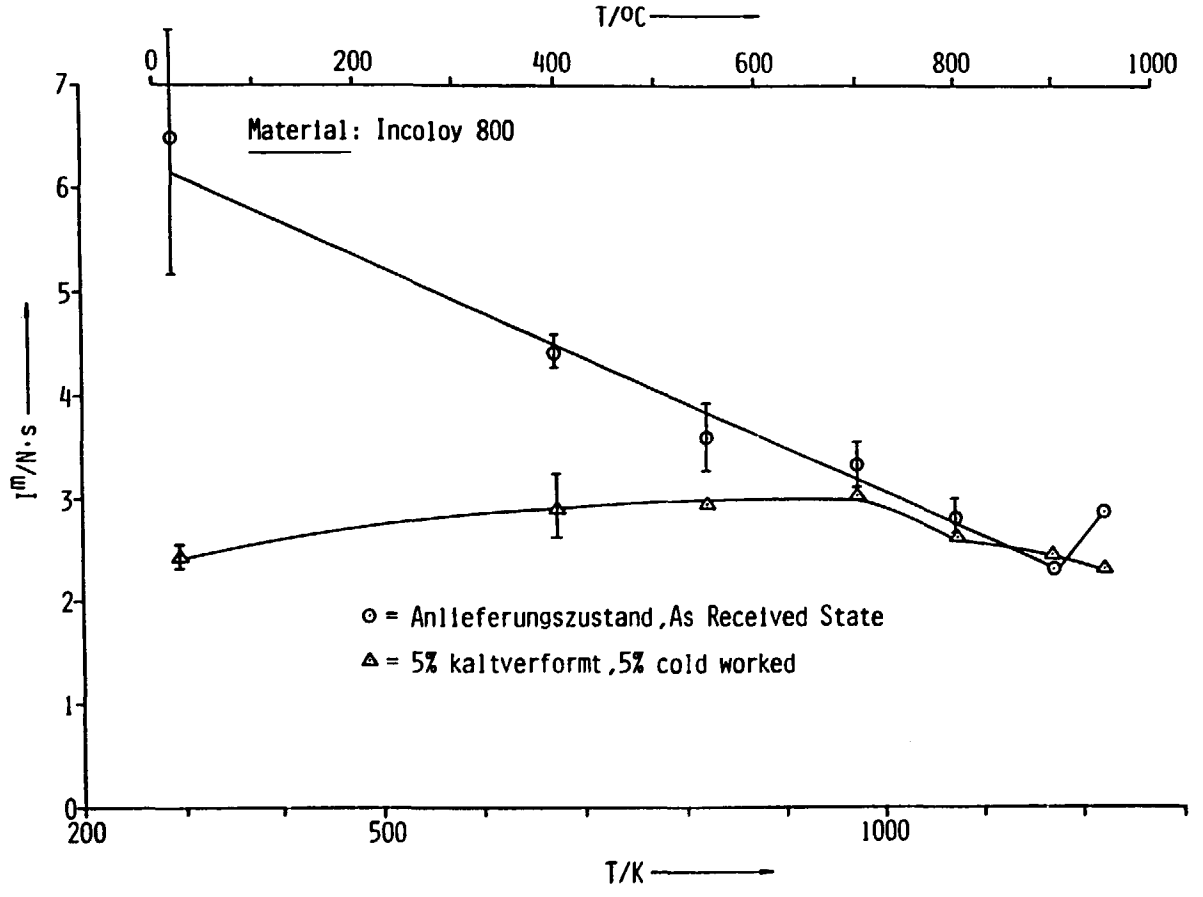

Fig. 12 Temperature Dependence of the Impulse up to the Load Maximum I^m for 10 % and 25 % cold-work

Abb. 12 Temperaturabhängigkeit des Impulses bis zum Lastmaximum I^m für 10 % und 25 % Kaltverformung

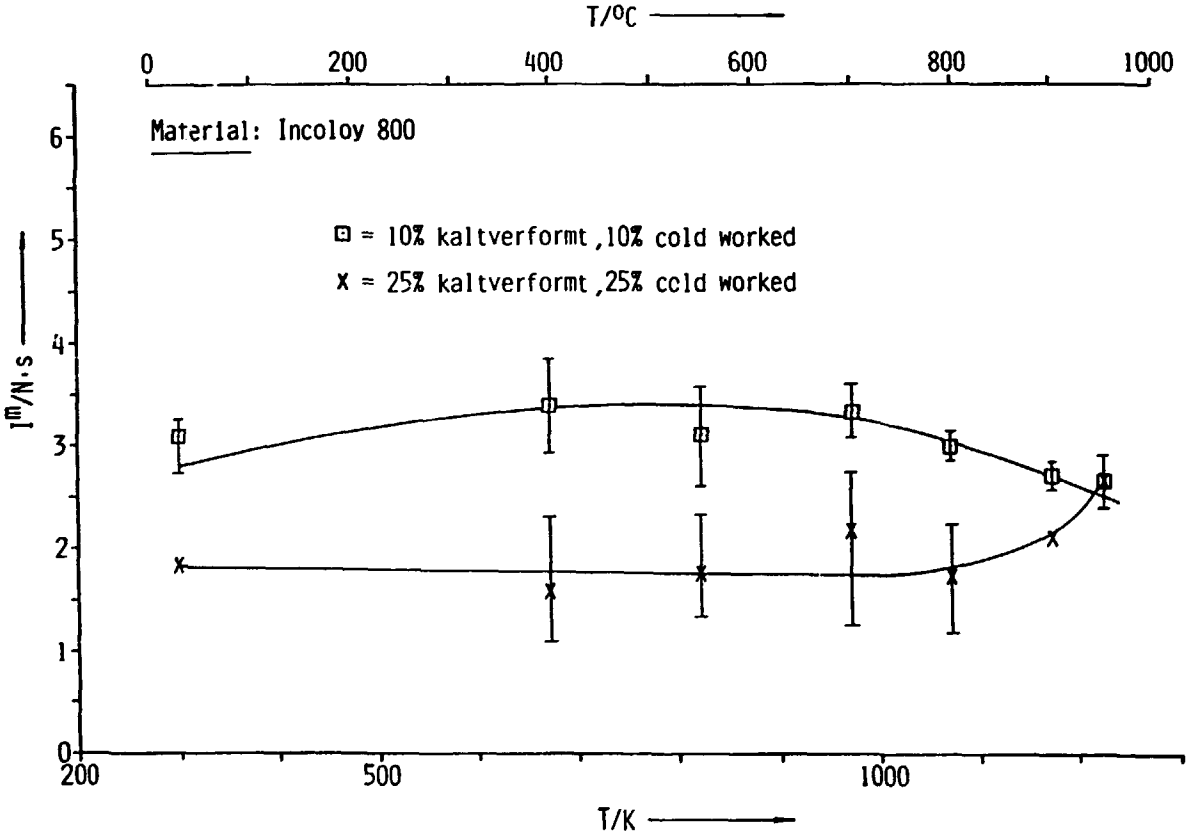

Fig. 13 Temperature Dependence of the dynamic Fracture Toughness K for the as-received state and 5 % cold-work

Abb. 13 Temperaturabhängigkeit der dynamischen Bruchzähigkeit K für den Anlieferungszustand und nach 5 % Kaltverformung

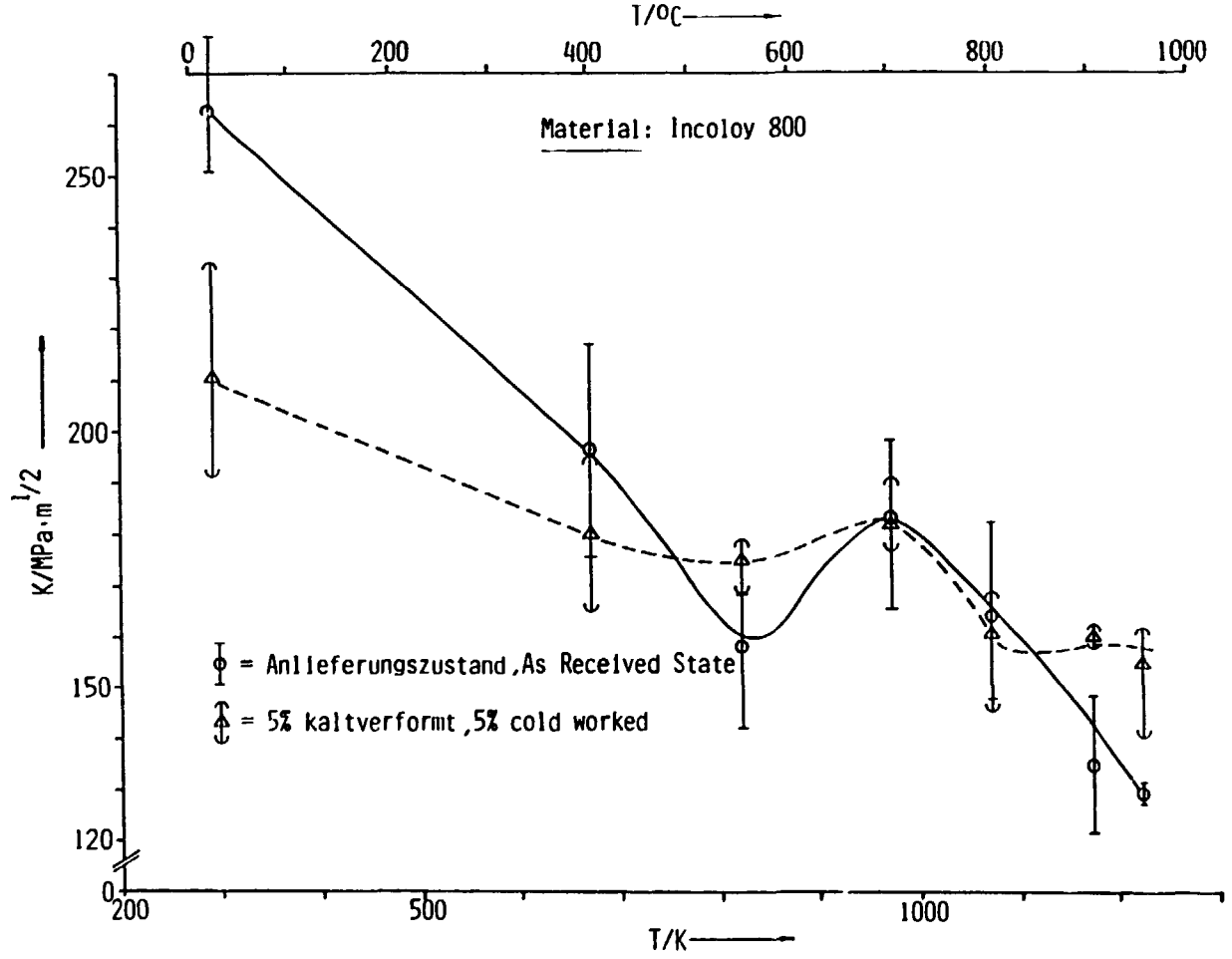

Fig. 14 Temperature Dependence of the dynamic Fracture Toughness K for 10 % and 25 % cold-work

Abb. 14 Temperaturabhängigkeit der dynamischen Bruchzähigkeit K nach 10 % und 25 % Kaltverformung

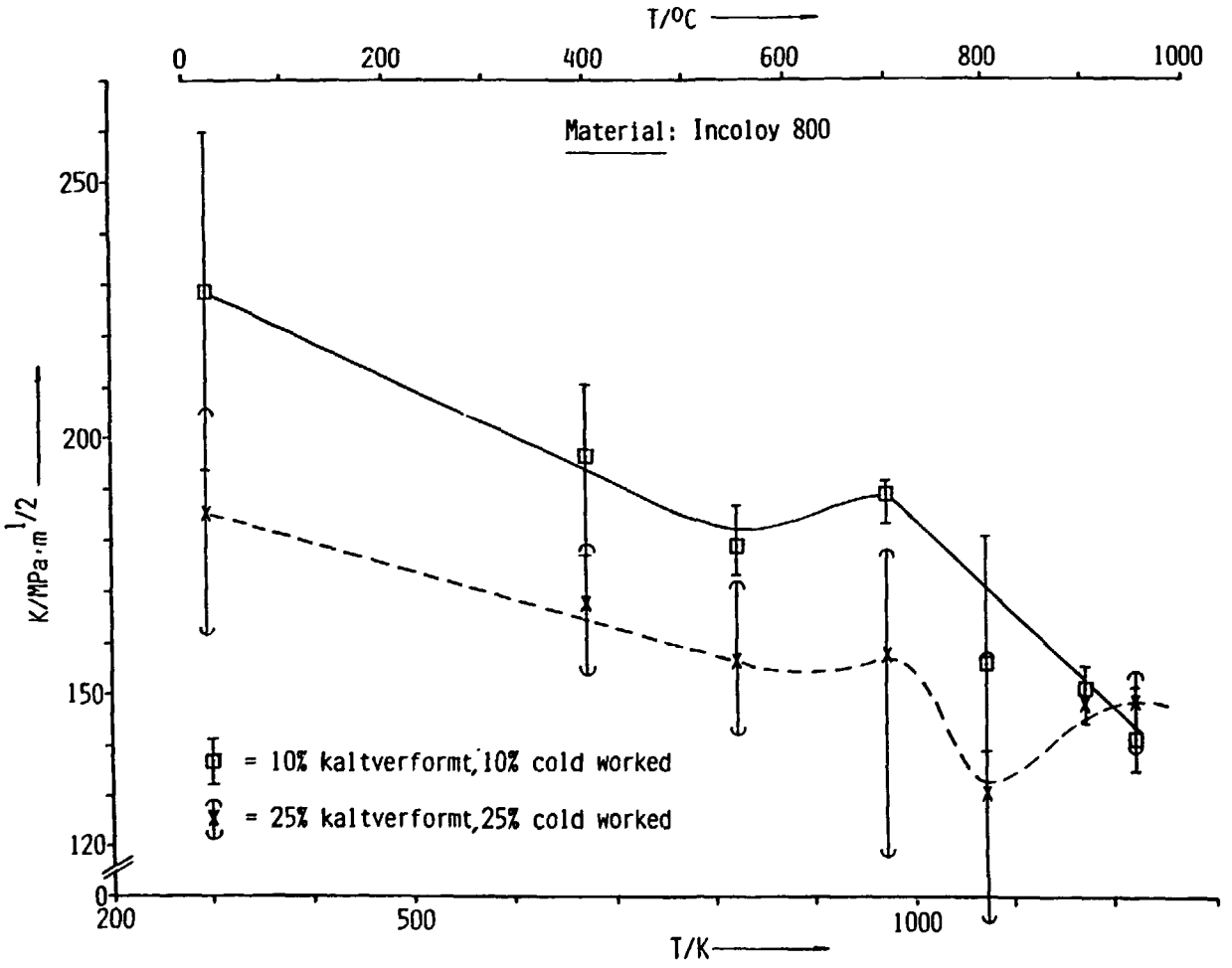

Fig. 15 Cold-work-Dependence of the normalized Impact Energies E, Isothermes

Abb. 15 Normalisierte Schlagenergie E in Abhängigkeit von der Kaltverformung, Isothermen

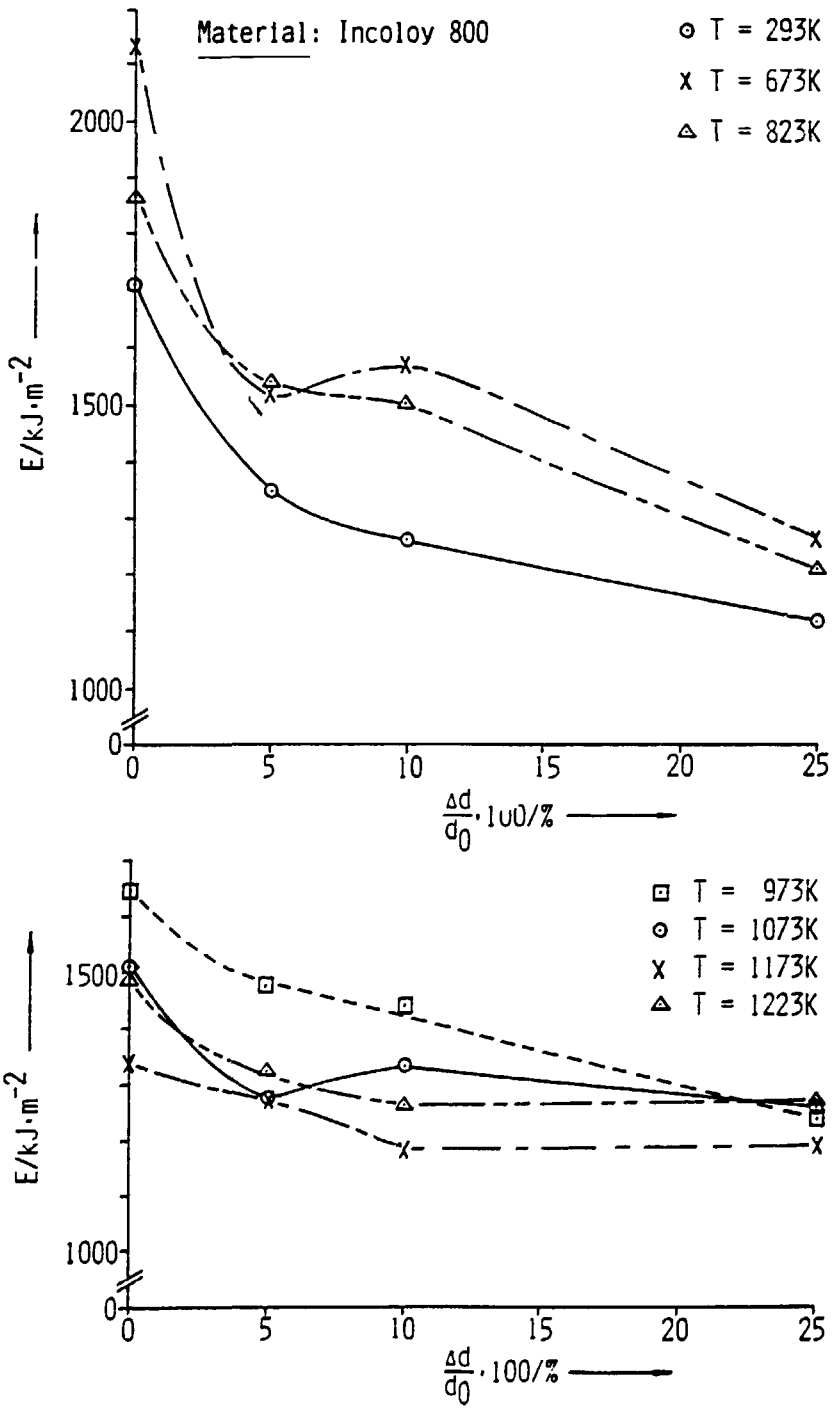

Fig. 16 Cold-Work-Dependence of the normalized Impact Energies up to the Load Maximum E^m, Isothermes

Abb. 16 Normalisierte Schlagenergie bis zum Lastmaximum E^m in Abhängigkeit von der Kaltverformung, Isothermen

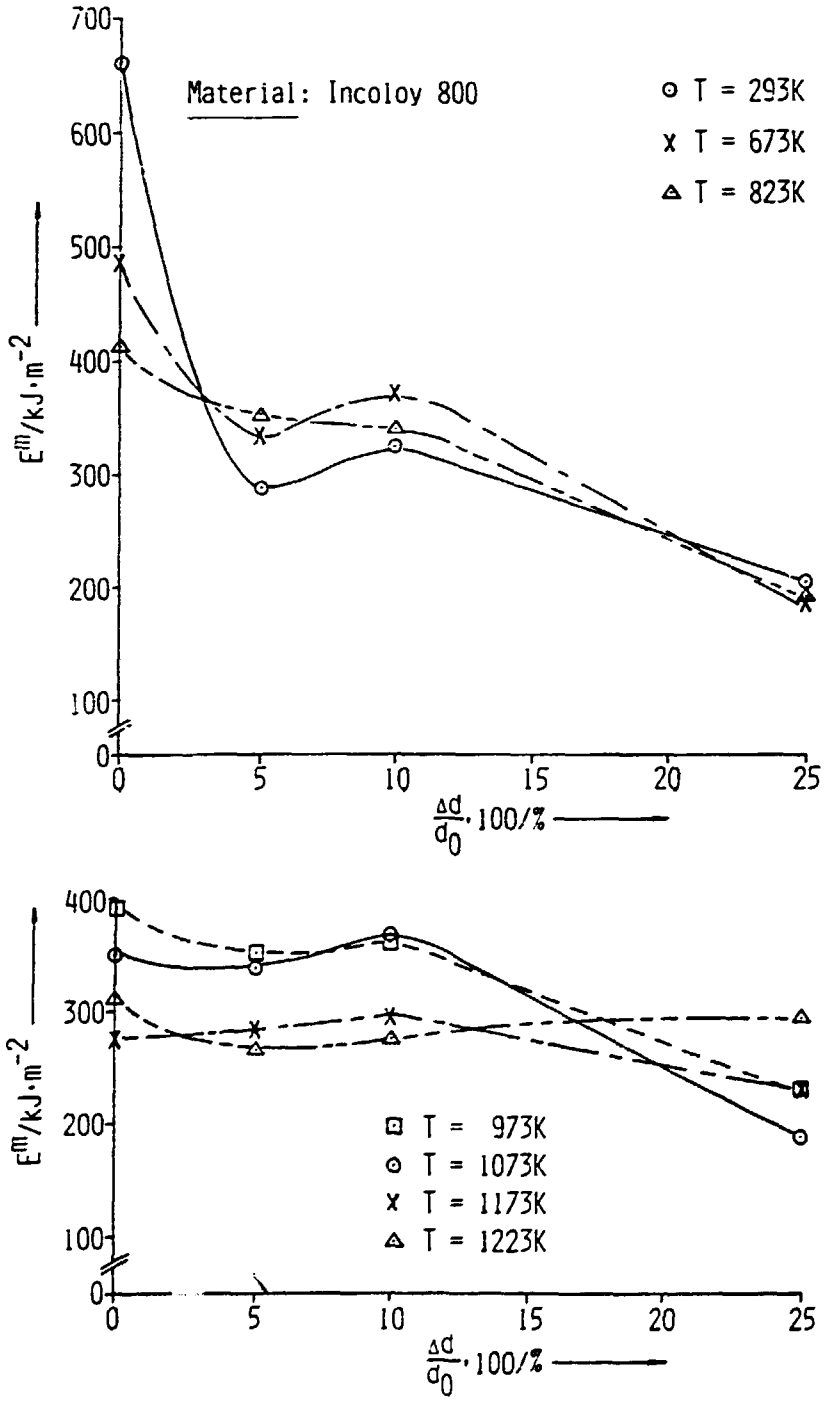

Fig. 17 Cold-Work-Dependence of the Impulse I, Isothermes

Abb. 17 Impuls I in Abhängigkeit von der Kaltverformung, Isotherme

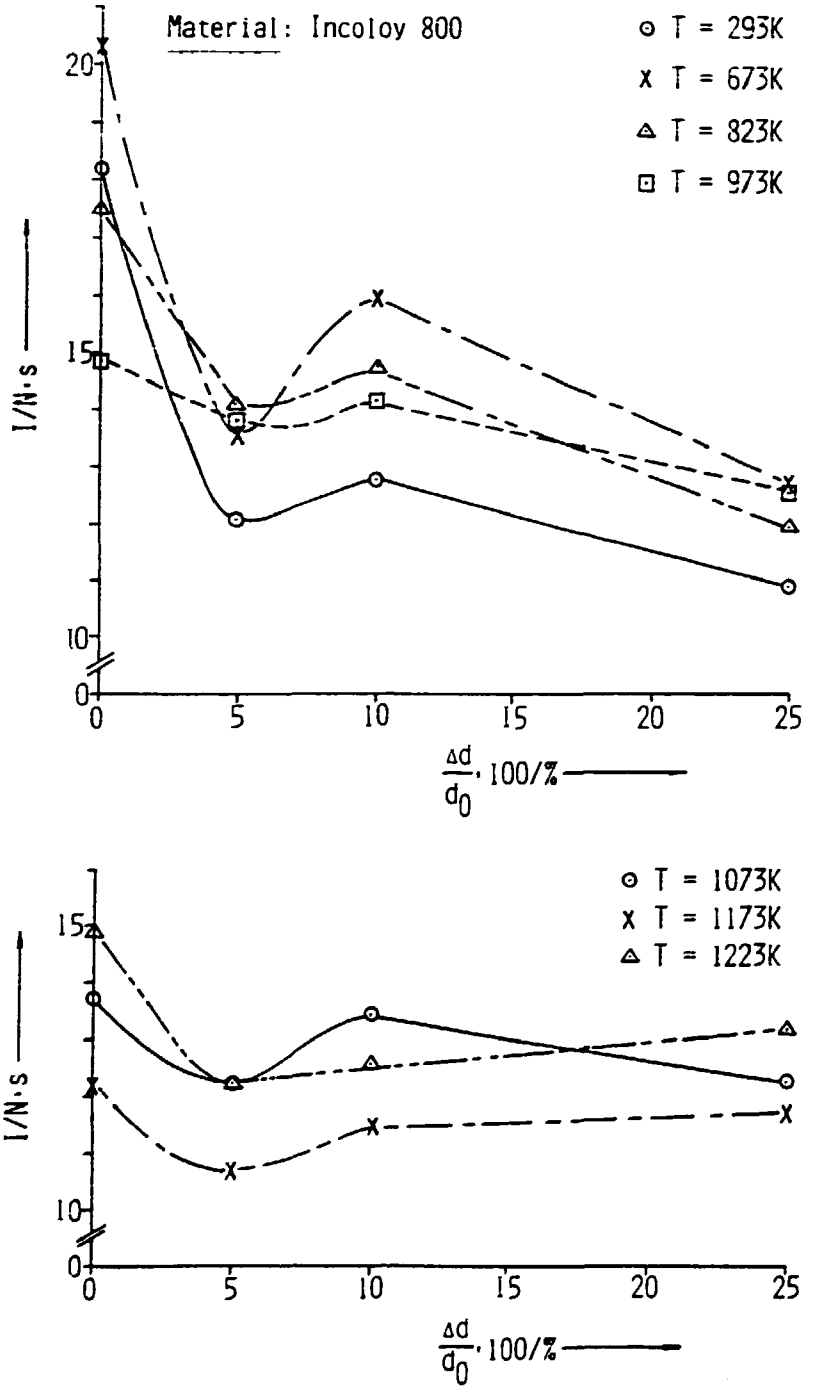

Fig. 18 Cold-Work-Dependence of the Impulse up to the Load Maximum I^m, Isothermes

Abb. 18 Impuls bis zum Lastmaximum I^m in Abhängigkeit von der Kaltverformung, Isotherme

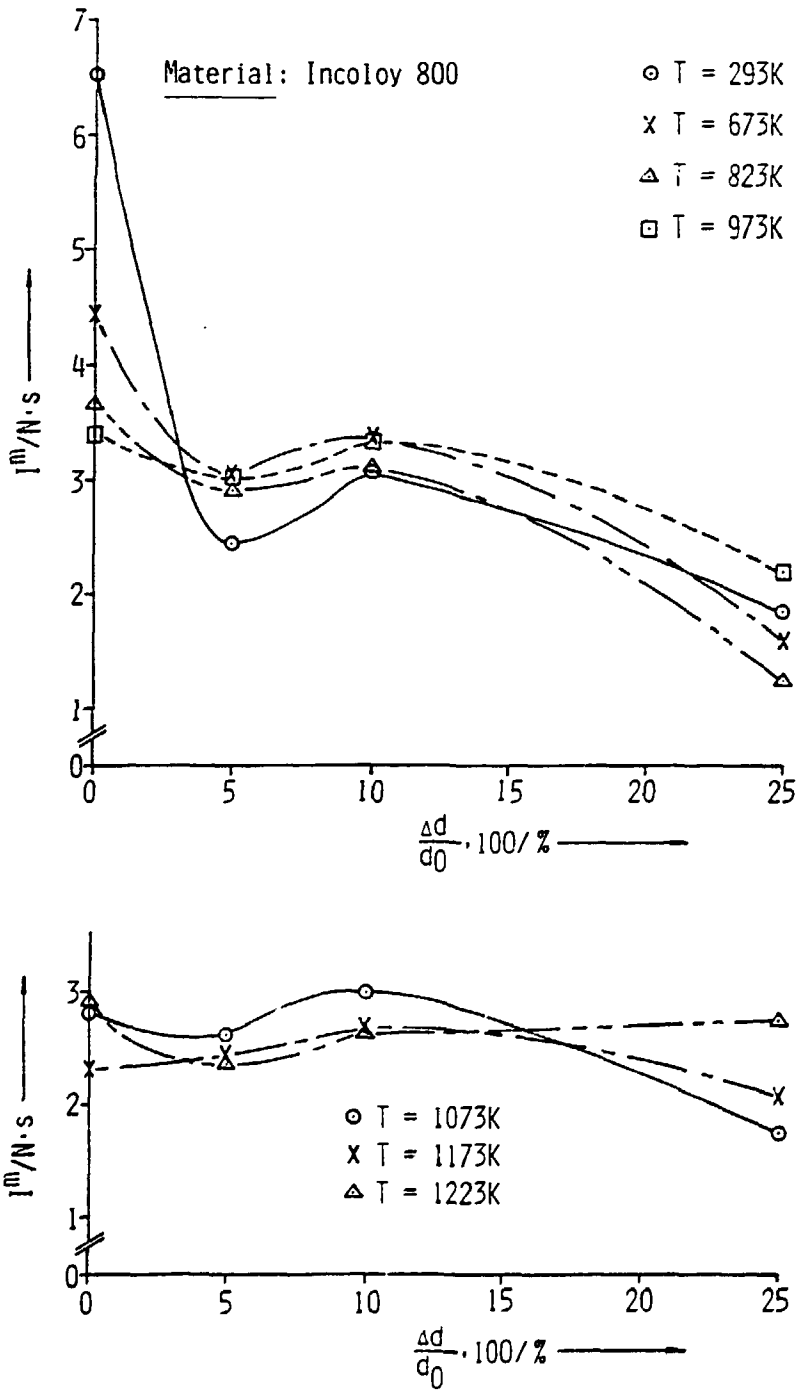

Fig. 19 Cold-Work-Dependence of the Fracture Toughness K, Isothermes
Abb. 19 Bruchzähigkeit K in Abhängigkeit von der Kaltverformung, Isotherme